3. Butler, R. P. & Marcy, G. W. A planet orbiting 47 Ursae Majoris. *Astrophys. J.* **464,** L153–L156 (1996).
4. Butler, R. P. *et al.* Three new "51 Peg-type" planets. *Astrophys. J.* **474,** L115–L118 (1997).
5. Cochran, W. D., Hatzes, A. P., Butler, R. P. & Marcy, G. W. The discovery of a planetary companion to 16 Cygni B. *Astrophys. J.* **483,** 5457–463 (1997).
6. Noyes, R. W. *et al.* A planet orbiting the star ρ Coronae Borealis. *Astrophys. J.* **483,** L111–L114 (1997).
7. Hatzes, A. P., Cochran, W. D. & Johns-Krull, C. M. Testing the planet hypothesis: a search for variability in the spectral line shapes of 51 Peg. *Astrophys. J.* **478,** 374–380 (1997).
8. Henry, G. W., Baliunas, S. L., Donahue, R. A., Soon, W. H. & Saar, S. H. *Astrophys. J.* **474,** 503–510 (1997).
9. Gray, D. F. Absence of a planetary signature in the spectra of the star 51 Pegasi. *Nature* **385,** 795–796 (1997).
10. Gray, D. F. & Hatzes, A. P. Nonradial oscillation in the solar-temperature star 51 Pegasi. *Astrophys. J.* **490,** 412–424 (1997).
11. Tull, R. G., MacQueen, P. J., Sneden, C. & Lambert, D. L. The high-resolution cross-dispersed echelle white pupil spectrometer of the McDonald Observatory 2.7-m telescope. *Publ. Astron Soc. Pacif.* **107,** 251–264 (1995).
12. Marcy, G. W. *et al.* The planet around 51 Pegasi. *Astrophys. J.* **481,** 926–935 (1997).

Acknowledgements. This work was supported by NASA's Origins of the Solar System Program.

Correspondence should be addressed to A.P.H. (e-mail: artie@astro.as.utexas.edu).

Kondo effect in a single-electron transistor

D. Goldhaber-Gordon*†, Hadas Shtrikman†, D. Mahalu†, David Abusch-Magder*, U. Meirav† & M. A. Kastner*

** Department of Physics, Massachusetts Institute of Technology, Cambridge, Massachussetts 02139, USA*

† Braun Center for Submicron Research, Department of Condensed Matter Physics, Weizmann Institute of Science, Rehovot 76100, Israel

How localized electrons interact with delocalized electrons is a central question to many problems in sold-state physics[1–3]. The simplest manifestation of this situation is the Kondo effect, which occurs when an impurity atom with an unpaired electron is placed in a metal[2]. At low temperatures a spin singlet state is formed between the unpaired localized electron and delocalized electrons at the Fermi energy. Theories predict[4–7] that a Kondo singlet should form in a single-electron transistor (SET), which contains a confined 'droplet' of electrons coupled by quantum-mechanical tunnelling to the delocalized electrons in the transistor's leads. If this is so, a SET could provide a means of investigating aspects of the Kondo effect under controlled circumstances that are not accessible in conventional systems: the number of electrons can be changed from odd to even, the difference in energy between the localized state and the Fermi level can be tuned, the coupling to the leads can be adjusted, voltage differences can be applied to reveal non-equilibrium Kondo phenomena[7], and a single localized state can be studied rather than a statistical distribution. But for SETs fabricated previously, the binding energy of the spin singlet has been too small to observe Kondo phenomena. Ralph and Buhrman[8] have observed the Kondo singlet at a single accidental impurity in a metal point contact, but with only two electrodes and without control over the structure they were not able to observe all of the features predicted. Here we report measurements on SETs smaller than those made previously, which exhibit all of the predicted aspects of the Kondo effect in such a system.

When the channel of a transistor is made very small and is isolated from its leads by tunnel barriers it behaves in an unusual way. A transistor can be thought of as an electronic switch that is on when it conducts current and off when it does not. Whereas a conventional field-effect transistor, such as one in a computer memory, turns on only once when electrons are added to it, the SET turns on and off again every time a single electron is added to it[9,10]. This increased functionality may eventually make SETs technologically important.

The unusual behaviour of SETs is a manifestation of the quantization of charge and energy caused by the confinement of the droplet of electrons in the small channel. As similar quantization occurs when electrons are confined in an atom, the small droplet of electrons is often called an artificial atom[11,12].

We have fabricated SETs using multiple metallic gates (electrodes) deposited on a GaAs/AlGaAs heterostructure (Fig. 1a) containing a two-dimensional electron gas, or 2DEG. First, the electrons are trapped in a plane by differences in the electronic properties of the heterostructure's layers. Second, they are excluded from regions of the plane beneath the gates when negative voltages are applied to

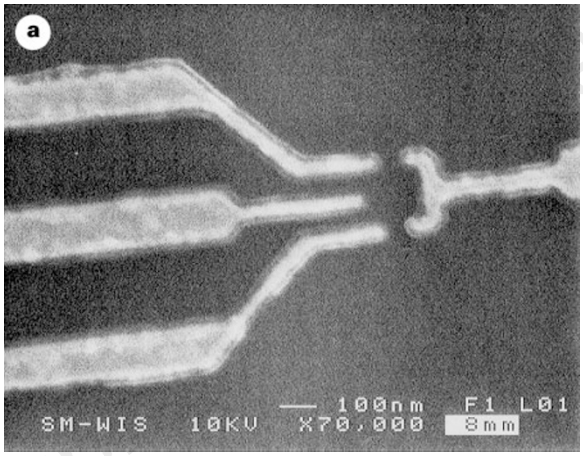

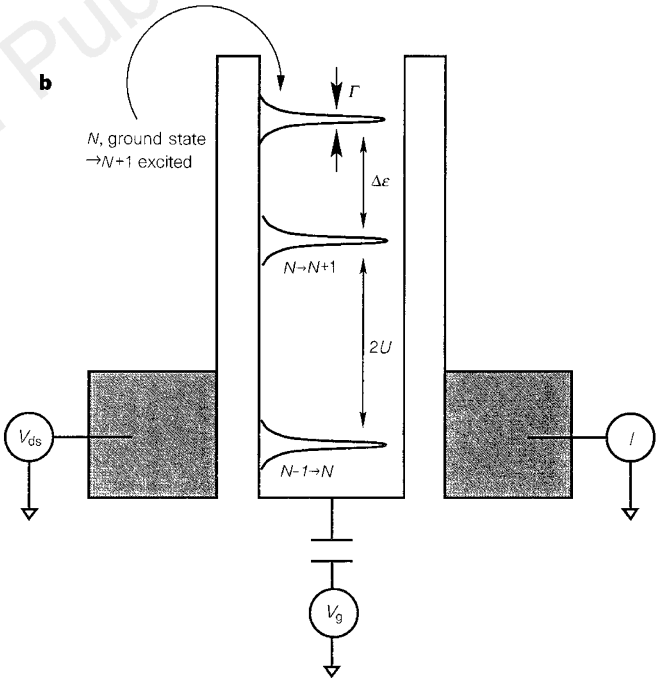

Figure 1 a, Scanning electron microscope image showing top view of sample. Three gate electrodes, the one on the right and the upper and lower ones on the left, control the tunnel barriers between reservoirs of two-dimensional electron gas (at top and bottom) and the droplet of electrons. The middle electrode on the left is used as a gate to change the energy of the droplet relative to the two-dimensional electron gas. Source and drain contacts at the top and bottom are not shown. Although the lithographic dimensions of the confined region are 150 nm square, we estimate lateral depletion reduces the electron droplet to dimensions of 100 nm square. The gate pattern shown was deposited on top of a shallow heterostructure with the following layer sequence grown on top of a thick undoped GaAs buffer: 5 nm $Al_{0.3}Ga_{0.7}As$, 5×10^{12} cm^{-1} Si δ-doping, 5 nm $Al_{0.3}Ga_{0.7}As$, δ-doping, 5 nm $Al_{0.3}Ga_{0.7}As$, 5 nm GaAs cap (H.S., D.G.-G. and U.M., manuscript in preparation). Immediately before depositing the metal, we etched off the GaAs cap in the areas where the gates would be deposited, to reduce leakage between the gates and the electron gas. **b**, Schematic energy diagram of the artificial atom and its leads. The situation shown corresponds to $V_{ds} < kT/e$, for which the Fermi energies in source and drain are nearly equal, and to a value of V_g near a conductance minimum between a pair of peaks corresponding to the same spatial state. For this case there is an energy cost $\sim U$ to add or remove an electron. To place an extra electron in the lowest excited state costs $\sim U + \Delta\epsilon$.

those gates. This creates a droplet of electrons separated from the leads by tunnel junctions. This basic technique has been used previously[13–17]. To make our SETs smaller than earlier ones, we have fabricated shallower 2DEG heterostructures (H.S., D.G.-G. and U.M., manuscript in preparation)[18] as well as finer metallic gate patterns by electron-beam lithography. The smaller size of the SETs is critical to our observation of the Kondo effect. (Dimensions are given in Fig. 1a.)

Several important energy scales and their relative sizes determine the behaviour of a SET (see Fig. 1b). At low temperature, the number of electrons N in the droplet is a fixed integer (roughly 50 for our samples). This number may be changed by raising the voltage of a nearby gate electrode which lowers the energy of electrons in the droplet relative to the Fermi level in the leads. The change in energy necessary to add an electron is called U, and in a simple model is the charging energy $e^2/2C$, where C is the capacitance of the droplet. As U is determined by the Coulomb repulsion between pairs of electrons in the droplet, it scales approximately inversely with the droplet's radius.

For small droplets, the quantized energy difference between different spatial electronic states becomes important. We call the typical energy spacing between spatial states $\Delta\epsilon$. Another important energy Γ is the coupling of electronic states on the artificial atom to those on the leads, resulting from tunnelling. When Γ is made greater than $\Delta\epsilon$, the electrons spread from the artificial atom into the leads, and quantization of charge and energy is lost, even at temperature $T = 0$.

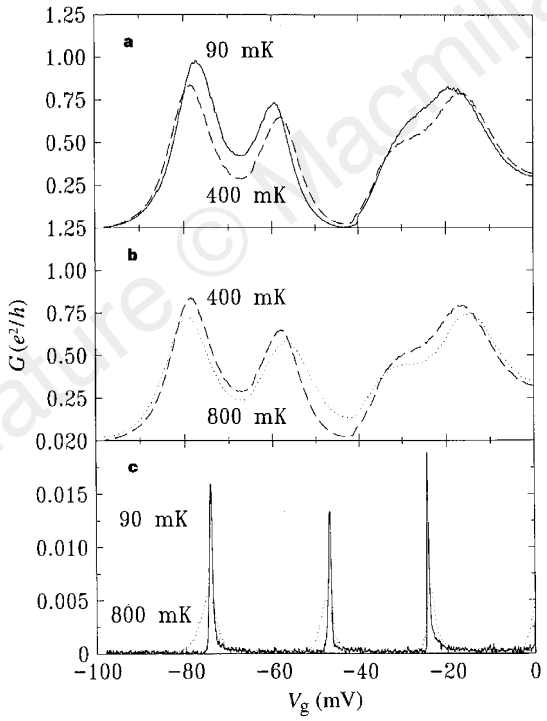

Figure 2 Temperature dependence of zero-bias conductance G through two different spatial states on the droplet. **a**, Paired peaks corresponding to the two spin states for each spatial state become better resolved with *increasing* temperature from 90 mK (full line) to 400 mK (dashed). The intra-pair valleys become deeper and the peaks become narrower. **b**, From 400 mK (dashed line) to 800 mK (dotted) the paired peaks near $V_g = -70$ mV broaden. The peaks near $V_g = -25$ mV are still becoming better resolved even at 800 mK, as they have larger Γ and hence larger T_K. **c**, When Γ is reduced (as illustrated by shorter and narrower peaks), U increases relative to $\Delta\epsilon$, so peak pairing is no longer evident. Because the Kondo phenomenon is suppressed, peaks become narrower as temperature is decreased at all T down to our base temperature of 90 mK. Full line is for 90 mK, dotted line for 800 mK.

Finally, the energy that determines whether Kondo physics will be visible is kT_K, which is always smaller than Γ. (Here k is Boltzmann's constant and T_K is called the Kondo temperature[7]. By making smaller SETs we have made $\Delta\epsilon$ relatively large, permitting large Γ and thus T_K comparable to accessible temperatures. In semiconductor SETs, Γ can be tuned by changing the voltage on the gates that create the barriers between artificial atom and leads. We find that with our new SETs we can vary Γ slowly as it approaches $\Delta\epsilon$, and thus optimize T_K.

In our experiment, we make two types of measurements. In the first, we apply a voltage of a few microvolts between the two leads to the SET, called the source and drain, and measure the current that flows through the droplet as a function of the voltage V_g on one of the SET's gates (the middle electrode on the left in Fig. 1a). For such low applied voltage ($<kT/e$), current varies linearly with voltage, and the zero-bias conductance can be measured. We use a 10 Hz a.c. excitation, and perform lock-in detection of the current. In the second class of measurements, we add a variable d.c. offset V_{ds} (up to several millivolts) to our a.c. excitation, and again use lock-in detection of current to obtain differential conductance dI/dV_{ds} against V_{ds}.

Varying V_g on a SET typically results in adding an electron to the droplet each time the voltage is increased by a fixed increment proportional to U. As current can flow through the SET only when the occupancy of the island is free to fluctuate between N and $N + 1$, a plot of conductance against V_g shows a series of sharp, periodically spaced peaks[15–17]. Figure 2c shows this behaviour when Γ is made relatively small. When Γ is large, as in Fig. 2a and b, we find that these peaks form pairs, with large inter-pair spacing and small intra-pair spacing. The two peaks within a pair have comparable widths and heights, whereas between pairs the widths vary significantly. These observations are direct evidence that two electrons of different spin are occupying each spatial state. Between paired peaks, N is odd, whereas between adjacent pairs it is even. As two electrons corresponding to the pair of peaks are added to the same spatial state, the intra-pair spacing is determined by U. However, when N is even (between pairs) the next electron must be placed in a different spatial state, so the interpair spacing is determined by $U + \Delta\epsilon$.

When $\Gamma \leq kT$ the peaks in conductance against gate voltage become narrower and larger with decreasing T, as illustrated in Fig. 2c, saturating at a width and height determined by Γ. This behaviour results from the sharpening of the Fermi distribution[15,18]. Figure 2 illustrates that this pattern is followed for large Γ, as well, on the outside edges of paired peaks at all T. However, inside pairs the peaks become narrower as T is reduced from 800 mK to 400 mK, but then broaden again at low temperatures, resulting in increased conductance in the intra-pair valley. Thus, not only the peak spacing but also the mechanism of conduction itself is different within pairs from between pairs. The enhancement of linear conductance at low temperature for odd but not even N is a manifestation of Kondo physics[19]. If N is odd there is an unpaired electron with a free spin which can form a singlet with electrons at the Fermi level in the leads. This coupling results in a greater density of states at the Fermi level of the leads, and hence higher conductance[4,5]. Raising the temperature destroys the singlet and attenuates the conductance.

Another aspect of the Kondo effect is the sensitivity of the excess conductance between the pair of peaks to the difference in Fermi levels in the two leads. The extra electron in the droplet couples to electrons in both leads, giving a greater density of states at both Fermi levels[7,20,21]. When the applied voltage is large, separating the Fermi levels in the two leads, the electrons at the Fermi level in the higher energy lead can no longer resonantly tunnel into the enhanced density of states in the lower energy lead, so the extra conductance is suppressed. This can be seen in Fig. 3, a plot of differential conductance against V_{ds}. The enhanced conductance is suppressed by a bias of $\sim$0.1 mV in either direction.

Figure 3 illustrates how this nonlinear conductance measurement

also offers a complementary way of seeing the suppression of the zero-bias enhancement with temperature. By 600 mK, the Kondo resonance has almost completely disappeared between the peak pair near $V_g = -70$ mV.

A magnetic field also alters the Kondo effect. Applying a magnetic field splits the unpaired localized electron state into a Zeeman doublet separated by the energy $g\mu_B B$. This also splits the enhanced density of states at the Fermi level into two peaks with energies $g\mu_B B$ above and below the Fermi level[7]. When the Fermi level of one lead is raised or lowered by a voltage $g\mu_B B/e$ relative to the other lead, electrons can tunnel into the Kondo-enhanced density of states. In differential conductance at high magnetic field, we thus see peaks at $\pm g\mu_B B/e$ (see Fig. 3). The splitting of peaks in differential conductance by *twice* $g\mu_B B$ (compared to the spin splitting of the localized state, $g\mu_B B$) provides a distinctive signature of Kondo physics. Because the peaks are broad and overlapping, measuring the distance between their maxima may underestimate their splitting at lower magnetic fields. At 7.5 T, when the peaks no longer overlap, we find their splitting to be 0.033 ± 0.002 meV T^{-1}. In comparison with measurements on bulk GaAs, this is significantly smaller than $2g\mu_B B$ yet larger than $g\mu_B B = 0.025$ meV T^{-1}. Electron spin resonance measurements have found[22] that spin splittings in a two-dimensional electron gas are suppressed compared with values for bulk samples, sometimes by as much as 35%. Thus, our measurement is consistent with a splitting of $2g\mu_B B$.

Figure 4 shows the differential conductance at low temperature and zero magnetic field as a function of both V_{ds} and V_g. This range of V_g spans the better-resolved pair of peaks near $V_g = -70$ mV in Fig. 2 as well as the valleys on either side of it. The bright diagonal lines result from strong peaks in dI/dV_{ds} (outside the range of V_{ds} shown in Fig. 3) marking the values of V_{ds} and V_g where N can change to $N+1$ or $N-1$. The slopes of these lines contain information about the relative capacitances of gates and leads to the droplet of electrons. Together with the intra-pair spacing of peaks in zero-bias conductance as a function of V_g at 800 mK (Fig. 2), these relative capacitances give a value for U of about 0.6 meV. The ratio $\Gamma/\Delta\epsilon$ is of order unity, so electron wavefunctions in the droplet extend somewhat into the leads, suppressing U. When Γ is reduced for this same device (as in Fig. 2c), U increases to ~2 meV. From the difference between inter- and intra-pair spacing in Fig. 2 we find $\Delta\epsilon \approx U$. To determine Γ, we set V_g so that the spatial state corresponding to the paired peaks is empty. Then the width of the peak in a plot of dI/dV_{ds} against V_{ds} corresponding to tunnelling into the empty state is the bare level width $\Gamma \approx 0.2$ meV. This is unmodified by Kondo-enhanced tunnelling, which can only occur when the state is singly occupied in equilibrium. All three quantities U, $\Delta\epsilon$ and Γ are considerably larger than $kT = 0.0078$ meV at base temperature.

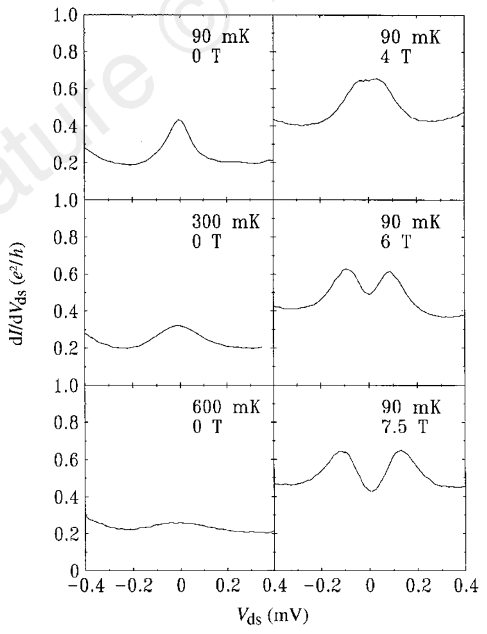

Figure 3 Temperature and magnetic field dependence of the zero-bias Kondo resonance measured in differential conductance. Increasing temperature suppresses the resonance, whereas increasing magnetic field causes it to split into a pair of resonances at finite bias. These scans were made with gate voltage halfway between the paired peaks near $V_g = -70$ mV in Fig. 2. Because the energy of the spatial state we are studying changes with magnetic field, the valley between our two peaks occurs at a different gate voltage for each value of magnetic field.

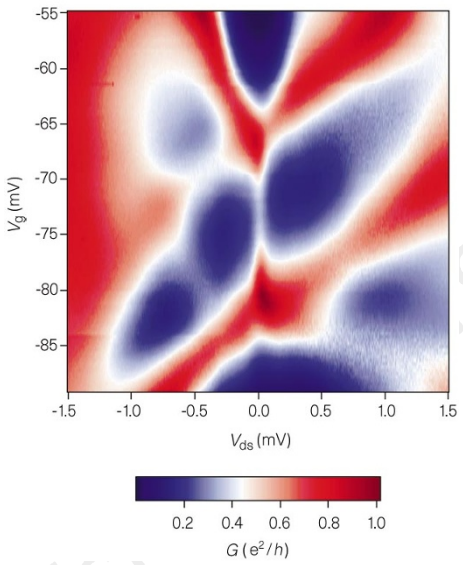

Figure 4 Differential conductance on a colour scale as a function of both V_g and V_{ds}. The white vertical line between the two maxima indicates that there is a zero-bias peak for odd N only.

A white vertical line at $V_{ds} = 0$ in Fig. 4 shows that the zero-bias conductance is enhanced everywhere between the paired peaks but not outside the pair. We find, in fact, that there is a zero-bias *suppression* just outside the pair, especially to the side towards negative gate voltage where our Kondo level is unoccupied[20]. The sharpness of the Kondo peak compared with other features is a dramatic illustration that we have, indeed, observed the Kondo effect in our SET. □

Received 29 July; accepted 14 October 1997.

1. Lawrence, J. M. & Mills, D. L. Recent progress in heavy fermion/valence fluctuation physics: Introduction. *Comments Cond. Mat. Phys.* **15,** 163–174 (1991).
2. Grüner, G. & Zawadowski, A. Magnetic impurities in non-magnetic metals. *Rep. Prog. Phys.* **37,** 1497–1583 (1974).
3. Varma, C. M. Mixed-valence compounds. *Rev. Mod. Phys.* **48,** 219–238 (1976).
4. Ng, T. K. & Lee, P. A. On-site Coulomb repulsion and resonant tunneling. *Phys. Rev. Lett.* **61,** 1768–1771 (1988).
5. Glazman, L. I. & Raikh, M. E. Resonant Kondo transparency of a barrier with quasilocal impurity states. *JETP Lett.* **47,** 452–455 (1988).
6. Meir, Y., Wingreen, N. S. & Lee, P. A. Low-temperature transport through a quantum dot: the anderson model out of equilibrium. *Phys. Rev. Lett.* **70,** 2601–2604 (1993).
7. Wingreen, N. S. & Meir, Y. Anderson model out of equilibrium: Noncrossing approximation approach to transport through a quantum dot. *Phys. Rev. B* **49,** 11040–11052 (1994).
8. Ralph, D. C. & Buhrman, R. A. Kondo-assisted and resonant tunneling via a single charge trap: a realization of the Anderson model out of equilibrium. *Phys. Rev. Lett.* **72,** 3401–3404 (1994).
9. Fulton, T. A. & Dolan, G. J. Observation of single-electron charging effects in small tunnel junctions. *Phys. Rev. Lett.* **59,** 109–112 (1987).
10. Meirav, U. & Foxman, E. B. Single-electron phenomena in semiconductors. *Semiconductor Sci. Technol.* **10,** 255–284 (1995).
11. Kastner, M. Artificial atoms. *Phys. Today* **46,** 24–31 (1993).
12. Ashoori, R. C. Electrons in artificial atoms. *Nature* **379,** 413–419 (1996).
13. van Wees, B. J. *et al.* Quantized conductance of point contacts in a two-dimensional electron gas. *Phys. Rev. Lett.* **60,** 848–851 (1988).
14. Wharam, D. A. *et al.* One-dimensional transport and the quantisation of the ballistic resistance. *J. Phys. C: Solid State Phys.* **21,** L209–214 (1988).
15. Meirav, U., Kastner, M. A. & Wind, S. J. Single-electron charging and periodic conductance resonances in GaAs nanostructures. *Phys. Rev. Lett.* **65,** 771–774 (1990).

16. Johnson, A. T. *et al.* Zero-dimensional states and single-electron charging in quantum dots. *Phys. Rev. Lett.* **69,** 1592–1595 (1992).
17. Weis, J., Haug, R. J., Klitzing, K. v. & Ploog, K. Competing channels in single-electron tunneling through a quantum dot. *Phys. Rev. Lett.* **71,** 4019–4022 (1993).
18. Foxman, E. B. *et al.* Crossover from single-level to multilevel transport in artificial atoms. *Phys. Rev. B* **50,** 14193–14199 (1994).
19. Wan, Y., Phillips, P. & Li, Q. Suppression of the Kondo effect in quantum dots by even–odd asymmetry. *Phys. Rev.* B **51,** R14782–14785 (1995).
20. König, J., Schmid, J., Schoeller, H. & Schön, G. Resonant tunneling through ultrasmall quantum dots: Zero-bias anomalies, magnetic-field dependence, and boson-assisted transport. *Phys. Rev. B* **54,** 16820–16837 (1996).
21. Hershfield, S., Davies J. H. & Wilkins, J. W. Probing the Kondo resonance by resonant tunneling through an Anderson impurity. *Phys. Rev. Lett.* **67,** 3720–3723 (1991).
22. Dobers, M., von Klitzing, K. & Weimann, G. Electron-spin resonance in the two-dimensional electron gas of GaAs–$Al_xGa_{1-x}As$ heterostructures. *Phys. Rev. Lett.* **38,** 5453–5456 (1988).

Acknowledgements. We thank G. Bunin for help with fabrication, N. Y. Morgan for help with measurements, and I. Aleiner, R. C. Ashoori, M. H. Devoret, D. Esteve, D. C. Glattli, A. S. Goldhaber, L. Levitov, K. Matveev, N. Zhitenev, and especially N. S. Wingreen and Y. Meir for discussions. This work was supported by the US Joint Services Electronics Program under contract from the Department of the Army, Army Research Office. D.G.-G. thanks the students and staff of the Weizmann Institute's Braun Center for Submicron Research for their hospitality during his stay there, and the Hertz Foundation for fellowship support. D.A.-M. thanks the Lucent Technologies Foundation for fellowship support.

Correspondence should be addressed to M.A.K. (e-mail: mkastner@mit.edu).

Metal–insulator transition induced by oxygen isotope exchange in the magnetoresistive perovskite manganites

N. A. Babushkina*, L. M. Belova*, O. Yu. Gorbenko†, A. R. Kaul†, A. A. Bosak†, V. I. Ozhogin* & K. I. Kugel‡

* *RRC Kurchatov Institute, 123182 Moscow, Russia*
† *Chemistry Department, Moscow State University, 119899 Moscow, Russia*
‡ *Scientific Center for Applied Problems in Electrodynamics, 127412 Moscow, Russia*

Perovskite manganites derived from $LaMnO_3$ have recently become the subject of intensive study following the discovery of 'colossal' magnetoresistance (a magnetically induced change in electrical resistance of up to several orders of magnitude) in several members of this family of compounds[1]. The manganites exhibit a broad range of electronic and magnetic phases, ranging from low-resistance ferromagnetic metals to high-resistance insulators, which are extremely sensitive to variation of composition[2], temperature and pressure[3]. A recent study showed that such sensitivity also extends to oxygen isotope exchange[4]: replacing ^{16}O with ^{18}O in $La_{0.8}Ca_{0.2}MnO_3$ produces an unusually large change in the magnetic properties (a 21-kelvin decrease in the Curie temperature). The magnitude of this isotope shift is evidence for the essential role played by electron–phonon coupling[5] in determining the transport properties of these materials. Here we show that this sensitivity to oxygen isotope exchange can be even more extreme. In its normal state, the compound $La_{0.175}Pr_{0.525}Ca_{0.3}MnO_3$ undergoes an insulator-to-metal transition as it is cooled below ~95 K. But we find that, after substituting ^{18}O for ^{16}O, the compound remains an insulator down to 4.2 K, so providing a vivid demonstration of the importance of lattice vibrations in these materials.

Here we consider the perovskite manganites $R_{1-x}M_xMnO_3$ (where R^{3+} is a rare earth cation, M is a doubly charged cation of large ionic radius, and both R and M fill A positions of ABO_3 perovskite lattice; ref. 1). In this system, colossal magnetoresistance (CMR) occurs in the temperature range of the phase transitions resulting in the formation of a ferromagnetic phase: only the ferromagnetic phase shows the metal-like conductivity. The most likely explanation of such behaviour relates the electrical conductivity to the strong intra-atomic spin coupling of t_{2g} and e_g electrons, and double exchange between neighbouring Mn^{3+} and Mn^{4+} ions assisted by $2p$ orbitals of O. At high temperatures, all $R_{1-x}M_xMnO_3$ phases are paramagnetic and semiconducting. With a decrease of temperature, a variety of phase transformations occurs depending on the doping level (x) and average ionic radius of the cations in the A position (r_A). In the range $x = 0.2–0.5$ the ferromagnetic transition takes place if the tolerance factor t (where $t = d_{A-O}/\sqrt{2}d_{Mn-O}$, and d denotes a interatomic distance) exceeds the critical value 0.91 as with $La_{1-x}Ca_xMnO_3$ (ref. 2); this value has been found empirically using Shannon ionic radii. The Mn–O bond length varies insignificantly with changes of R and M at the constant Mn^{4+}/Mn^{3+} ratio, whereas the A–O bond length is a function of r_A. MnO_6 octahedra forming a three-dimensional array in the perovskite structure can be considered nearly invariant. These octahedra tilt and rotate to follow the reduction of space around the A cation if t decreases[2]. This buckling results in a decrease of the Mn–O–Mn bond angle θ, which disrupts the overlapping of $2p$ orbitals of O and e_g orbitals of Mn ions. If the overlapping is insufficient, then double exchange is no longer possible in Mn–O–Mn chains. The localized holes at e_g orbitals tend to lead to the formation of a charge-ordered (CO) state of the type found in $La_{0.5}Ca_{0.5}MnO_3$ (ref. 6); the material also becomes antiferromagnetic. Such a situation occurs in $Pr_{1-x}Ca_xMnO_3$ ($t < 0.91$ for $x = 0.2–0.4$), which has been intensively studied[7,8].

The behaviour mentioned above suggests that, besides double exchange, the electron–phonon coupling must play an essential role in the CMR manganites. For instance, the stretching vibration of the Mn–O–Mn chain would change angle θ (which controls the double exchange) and consequently the electrical conductivity of the chain. For $t \approx 0.91$, one can imagine a material which still has metal-like conductivity owing to the stretching vibration, where the angle θ periodically reaches a sufficient value for effective double exchange. If one suppresses the vibration, then the material under study is expected to become a CO insulator. We therefore considered the possibility of producing a pronounced variation of the electrical conductivity by substitution of ^{18}O for ^{16}O in $R_{1-x}M_xMnO_3$ at $t \approx 0.91$ owing to the strong electron–phonon coupling. For the first time, a 21 K decrease of the Curie temperature T_C after isotope exchange $^{18}O \rightarrow {}^{16}O$ has been reported by Zhao *et al.*[4] for $La_{0.8}Ca_{0.2}MnO_3$ with $t \approx 0.92$. For compositions with higher t the isotope effect was less profound; in the case of $La_{0.945}Mn_{0.945}O_3$, a T_C shift of ~12 K was observed[9]. These results suggest that a stronger oxygen isotope effect could be obtained by decreasing t.

The system $(La_{1-y}Pr_y)_{0.7}Ca_{0.3}MnO_3$ should be suitable for testing this approach to the production of a strong isotope effect. On the one hand, in this series of solid solutions t passes through critical value 0.91. Starting at ~260 K for $La_{0.7}Ca_{0.3}MnO_3$, both T_C and maximum resistivity temperature (T_p) decrease rapidly with increasing Pr content: $Pr_{0.7}Ca_{0.3}MnO_3$ is a CO insulator. On the other hand, $(La_{1-y}Pr_y)_{0.7}Ca_{0.3}MnO_3$ is a convenient system to work with because the oxygen stoichiomery is rather insensitive to variations of the heat treatment (temperature and partial pressure of O_2)[2]. So the Mn^{4+}/Mn^{3+} ratio is constant in the series. The isotope effect observed by us for the composition $La_{0.175}Pr_{0.525}Ca_{0.3}MnO_3$ has been far in excess of our expectations, as not merely a shift of T_p but also a metal–insulator transition due to the isotope exchange was established.

To prepare ceramic samples, aqueous solutions of $La(NO_3)_3$, $Pr(NO_3)_3$, $Ca(NO_3)_2$ and $Mn(NO_3)_2$ were mixed together in the proper ratio, and ash-free paper filters were soaked with the solution. The paper was dried at 120 °C and then burned: the product was annealed at 700 °C for 2 h. Pellets pressed from the powder residue were sintered at 1,200 °C for 12 h in air. Ceramics of composition $La_{0.175}Pr_{0.525}Ca_{0.3}MnO_3$ were obtained, and were found to be single phase according to X-ray diffraction with orthorhombic lattice parameters $a = 0.5436(2)$ nm, $b = 0.5461(2)$ nm, $c = 0.7686(3)$ nm at 300 K.